

Perceive, Understand and Restore: Real-World Image Super-Resolution with Autoregressive Multimodal Generative Models

Hongyang Wei^{1,3,*}, Shuaizheng Liu^{2,3,*}, Chun Yuan^{1,†}, Lei Zhang^{2,3,†}
¹Tsinghua Shenzhen International Graduate School, Tsinghua University
²The Hong Kong Polytechnic University ³OPPO Research Institute
 weihy23@mails.tsinghua.edu.cn, shuaizhengliu21@gmail.com
 yuanc@sz.tsinghua.edu.cn, cslzhang@comp.polyu.edu.hk

Abstract

By leveraging the generative priors from pre-trained text-to-image diffusion models, significant progress has been made in real-world image super-resolution (Real-ISR). However, these methods tend to generate inaccurate and unnatural reconstructions in complex and/or heavily degraded scenes, primarily due to their limited perception and understanding capability of the input low-quality image. To address these limitations, we propose, for the first time to our knowledge, to adapt the pre-trained autoregressive multimodal model such as Lumina-mGPT into a robust Real-ISR model, namely **PURE**, which **P**erceives and **U**nderstands the input low-quality image, then **R**estores its high-quality counterpart. Specifically, we implement instruction tuning on Lumina-mGPT to perceive the image degradation level and the relationships between previously generated image tokens and the next token, understand the image content by generating image semantic descriptions, and consequently restore the image by generating high-quality image tokens autoregressively with the collected information. In addition, we reveal that the image token entropy reflects the image structure and present an entropy-based Top-k sampling strategy to optimize the local structure of the image during inference. Experimental results demonstrate that **PURE** preserves image content while generating realistic details, especially in complex scenes with multiple objects, showcasing the potential of autoregressive multimodal generative models for robust Real-ISR. The model and code will be available at <https://github.com/nonwhy/PURE>.

* Equal Contribution.

† Corresponding Authors. This work is supported by the PolyU-OPPO Joint Innovative Research Center.

1. Introduction

Real-world image super-resolution (Real-ISR) is a challenging task in computer vision, aiming to reconstruct high-quality (HQ) images from low-quality (LQ) inputs degraded by complex combinations of factors such as blur, noise, downsampling, *etc.* Traditional discriminative image restoration methods [6, 8, 18, 19, 49] are typically designed for optimizing image fidelity using L_1 or L_2 losses, tending to produce over-smoothed results. While generative adversarial network (GAN [10])-based approaches [15, 35] can generate more visually appealing details, they suffer from unstable training and unnatural visual artifacts.

The recently developed large-scale pre-trained text-to-image (T2I) generation models, such as Stable Diffusion (SD) [1], have enabled more effective modeling of the complex distribution of natural images, and researchers have proposed to leverage the powerful T2I generative priors to achieve more perceptually realistic Real-ISR outcomes. Many SD-based methods [20, 33, 40, 44] adopt a ControlNet [47] architecture, extracting features from the LQ image as control signals to guide the generation of HQ image from random noise. Meanwhile, methods have also been proposed to extract semantic information, such as tags [40], short captions [43] and long descriptions [44], from the LQ image to help the SD model synthesizing more visual details. One-step diffusion-based Real-ISR methods [4, 28, 39] have also been proposed, which directly take the LQ image as input and finetune the SD model using LoRA [12] techniques.

Despite the significant progress achieved in SD-based Real-ISR, the existing models exhibit certain limitations, particularly in handling complex scenes with multiple objects or severe degradation. First, they may lack global understanding of the image content, leading to the generation of semantically inaccurate details. As shown in Fig. 1a, the state-of-the-art models SeeSR [40] and OSEDiff [39] misidentify buildings as cliffs, leading to incorrect restora-

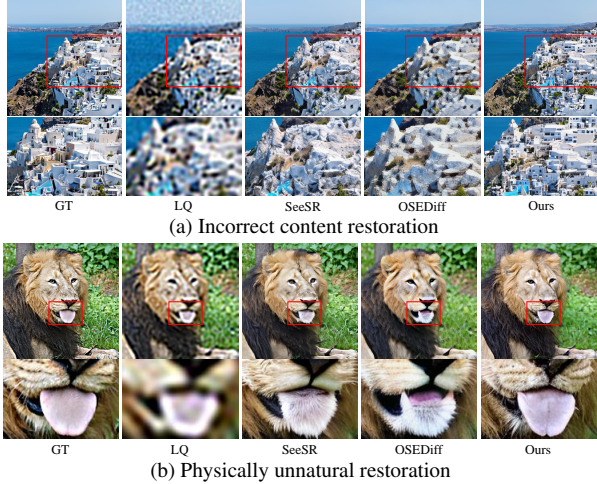


Figure 1. Examples of (a) inaccurate and (b) unnatural restoration of current SD-based Real-ISR methods, such as SeeSR[40] and OSEDiff [39], in complex and heavily degraded scenes.

tion of the scene. Second, existing models lack strong perception of the local structural relationships in natural images, leading to semantically coherent but physically unnatural appearance. As shown in Fig. 1b, SeeSR and OSEDiff erroneously synthesize the lion’s tongue with fur. These limitations highlight the need for a new Real-ISR model, which can simultaneously perceive, understand and restore the image with complex contents.

The recent advances in autoregressive multimodal large language models (MLLMs) [21, 22, 30, 41, 50] may offer a promising solution to the above-mentioned problem. Leveraging the large-capacity network trained on extensive multimodal datasets, these models excel at modeling the joint distribution of texts and images, integrating image understanding and generation within a unified framework, while the autoregressive generation process can model the image local structure relationships, providing a strong prior for local structure perception. Based on these facts, we present a framework, namely **PURE**, to **P**erceive, **U**nderstand, and **R**Estore the HQ image from its LQ observation by fine-tuning a pre-trained MLLM.

Specifically, by taking the LQ image as input, we implement instruction tuning on the Lumina-mGPT [21] to predict image degradation characteristics, semantic descriptions, and consequently the HQ output within a single model. On the one hand, our model can effectively utilize the perceived image degradation and semantic understanding features during the image generation process. On the other hand, the autoregressive generation process can explicitly consider the relationships between previously generated image tokens and the next tokens to be generated, alleviating the issue of physically unnatural appearance. Furthermore, we propose an entropy-based Top- k sampling strategy, which adaptively chooses the optimal Top- k value

based on the entropy during inference, further optimizing the local structure preservation.

Our contributions are summarized as follows. First, we propose, for the first time to our best knowledge, an autoregressive multimodal learning framework, which integrates global understanding and local perception, for robust Real-ISR. Second, we develop an entropy-based Top- k sampling strategy during inference to better preserve image structures while generating realistic details. Finally, our experimental results demonstrate the potential of PURE for Real-ISR tasks, particularly in complex scenarios.

2. Related Work

Real-World Image Super-Resolution. Traditional Real-ISR methods [6, 8, 18, 19, 49] typically adopt discriminative networks trained with pixel-wise L_1 or L_2 losses to recover high-frequency details, but often produce over-smoothed results. To improve perceptual quality, GAN-based approaches [15, 35] leverage adversarial losses to synthesize realistic textures, albeit at the cost of unstable training and artifacts. Recent advances focus on exploiting pre-trained text-to-image (T2I) diffusion models, such as SD [1], as generative priors. Some methods employ a ControlNet-based architecture [47] to guide SD generation using LQ image features as conditional signals, while some other methods enhance semantic alignment by extracting text descriptions [43, 44] or tags [40] from LQ inputs. One-step diffusion variants [4, 28, 39] further accelerate inference by directly mapping LQ to HQ images through LoRA-finetuned SD-UNet. Despite improved perceptual quality, these methods struggle with semantic inaccuracies and unnatural local structures in complex scenes due to limited global understanding and local relationship modeling.

Multimodal Large Language Models. Recent advancements in MLLMs [21, 22, 30, 41, 50] have expanded the capabilities of traditional language models to process and generate cross-modal content. Early works, such as LLaVA [22] and BLIP [16], focused on enhancing multimodal understanding by aligning pretrained vision encoders (*e.g.*, CLIP [24]) with LLMs like LLaMA [31], enabling tasks such as visual question answering and image captioning. However, these models primarily emphasized perception, lacking native generative abilities for visual content. To address multimodal generation, approaches like Show-o [41] and Transfusion [50] integrate autoregressive text modeling with diffusion-based image decoders (*e.g.*, SD), where the LLM predicts text tokens and relies on external diffusion models to synthesize images. Although effective, this hybrid paradigm introduces dependency on separate generative frameworks, leading to inconsistent outputs and limited end-to-end learning. In contrast, unified understanding and generation is pioneered by multimodal models such as Chameleon [30], Lumina-mGPT [21] and Emu3 [36],

which treat images as discrete tokens within an autoregressive framework, enabling seamless multimodal sequence modeling for text and images. In this work, we employ Lumina-mGPT as the MLLM for Real-ISR tasks.

3. Method

3.1. Preliminaries

Chameleon [30] is a representative MLLM, which uses next-token prediction in a discrete space to handle texts and images. Lumina-mGPT [21] further enhances Chameleon by enabling photorealistic text-to-image generation through supervised fine-tuning. In our work, we leverage Lumina-mGPT as the base model for Real-ISR, leveraging its strong image synthesis and understanding priors.

Vision Tokenizer. Lumina-MGPT [21] unifies vision-language understanding and generation through a VQGAN-based [9] tokenizer, which converts continuous images into symbolic sequences. It integrates three functional components: an encoder compressing visual inputs with down-sampling factor f , a quantizer discretizing latent vectors by nearest-codebook matching with size N , and a decoder reconstructing images from token-codebook mappings. In Real-ISR, the tokenizer will directly impact reconstruction quality: lower f preserves spatial details by reducing compression, while larger N enhances feature expressiveness through fine-grained codebook representations.

Training. Multimodal large language models process concatenated text-image token sequences through autoregressive learning. The objective maximizes the likelihood of target sequence $\mathbf{y} = \{y_1, \dots, y_T\}$ via conditional probability factorization $P(\mathbf{y}|\mathbf{x}) = \prod_{t=1}^T P(y_t|\mathbf{c}_{<t}, \mathbf{x})$, where $\mathbf{c}_{<t} = \{y_1, \dots, y_{t-1}\}$ denotes preceding context, and \mathbf{x} represents conditional inputs (e.g., low-quality images). Optimization minimizes stepwise CrossEntropy between predictions and targets: $\mathcal{L} = \text{CrossEntropy}(P(y_t|\mathbf{c}_{<t}, \mathbf{x}), y_t)$.

Inference. Autoregressive generation samples tokens $y_t \sim P(y_t|\mathbf{c}_{<t}, \mathbf{x})$ sequentially. To balance diversity and quality, Top- k sampling truncates the k -highest candidates before renormalization $y_t \sim P_{\text{Top-}k}(y_t|\mathbf{c}_{<t}, \mathbf{x})$, where hyperparameter $k \in \mathbb{Z}^+$ governs the candidate pool size.

3.2. Architecture of PURE

To address the issue that SD-based Real-ISR models tend to generate inaccurate and unnatural reconstructions in complex and/or heavily degraded scenes, we propose PURE, a robust Real-ISR framework based on autoregressive multimodal generative models. As illustrated in Fig. 2, our model architecture comprises three core components: a text tokenizer, a vision tokenizer, and a decoder-only Transformer backbone. The Transformer we employed primarily follows the design principles of Lumina-mGPT, which consists of RMSNorm [45] and QK-Norm [30] for normalization,

SwiGLU [26] as the activation function, and rotary positional embeddings (RoPE) [27] for positional encoding.

As discussed in Sec. 3.1, the vision tokenizer plays a critical role in extracting discrete latent representations of visual inputs, while its quality directly impacts the performance of downstream vision tasks. Although Lumina-mGPT utilizes a VQGAN with f of 16 and N of 8,192, allowing it to encode a 512×512 image into a sequence of 1,024 discrete tokens, the high compression ratio and limited codebook capacity lead to substantial information loss during the extraction of discrete image representations. This loss is particularly detrimental to image restoration tasks, where preserving fine-grained image structure and details is critical. To mitigate this issue, we propose to adopt a more advanced vision tokenizer. Specifically, we employ the VQGAN introduced in LlamaGen [29], which features a reduced f of 8 and an expanded N of 16,384. This configuration can significantly reduce information loss during encoding, thereby enhancing the quality of reconstructed images in our Real-ISR task.

For the text tokenizer, we retain the Byte Pair Encoding (BPE) tokenizer [30] from Lumina-mGPT with a vocabulary size of 65,536. Since the vocabulary includes image codebook tokens, expanding VQGAN’s codebook size needs a corresponding expansion in BPE tokenizer’s vocabulary. We therefore expand the vocabulary size from 65,536 to 73,728 to accommodate the additional discrete image tokens. To accommodate the expanded VQGAN codebook and BPE tokenizer vocabulary, we resize the model’s embedding layer (which maps discrete symbols to continuous vector representations), the output layer, and a classification head that predicts distributions over the vocabulary.

3.3. Training of PURE

As illustrated in Fig. 2, PURE takes the instruction and an LQ image as inputs and sequentially outputs degradation levels, semantic descriptions, and HQ results. Specifically, given an LQ image, the pipeline is guided by the following instruction: “*Perceive the degradation level, understand the image content, and restore the high-quality image.*” This instruction is first processed by a text tokenizer, converting it into discrete text tokens. Simultaneously, the LQ image is transformed into discrete image tokens via a vision tokenizer. Both sets of tokens are fed into the network as inputs, enabling the model to execute the sequential tasks of perception, understanding, and restoration.

Perception. The perception module initiates the pipeline by quantitatively analyzing the degradation of the input LQ image. We employ a Degradation Estimation module (DEM) in MM-RealSR+ [23], which evaluates the degradation of the LQ image and assigns scores for both noise and blur. These scores are categorized into three discrete levels: small, medium, and large, which are then explicitly encoded

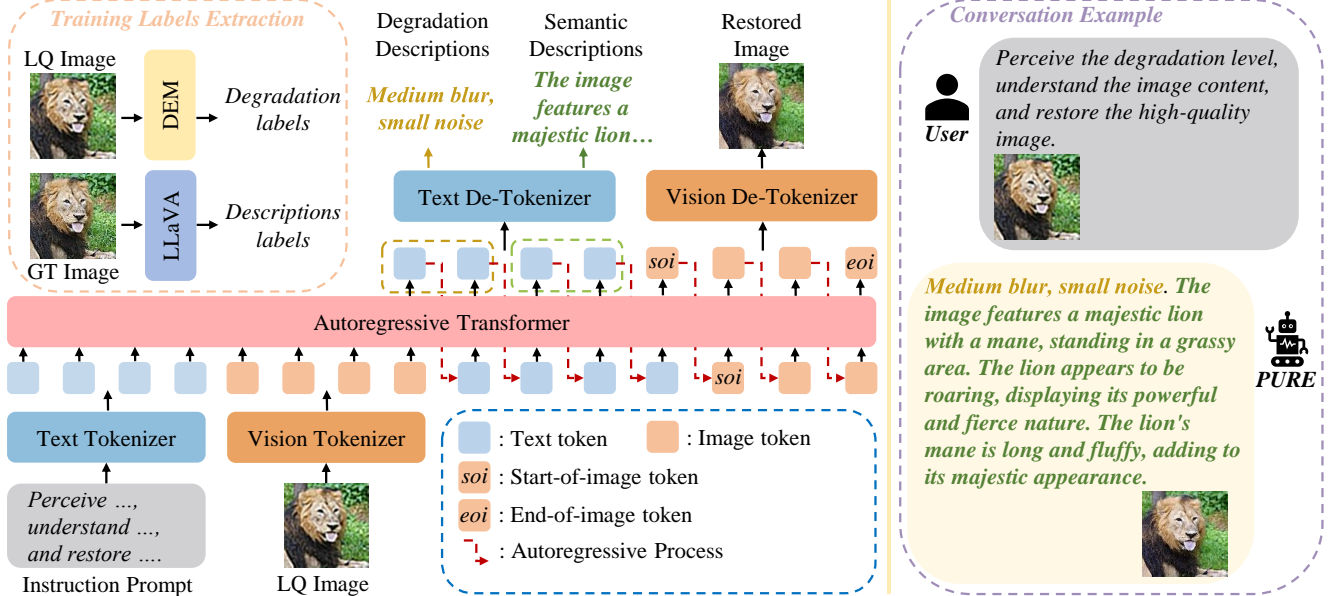


Figure 2. Overview of PURE. We utilize VQGAN’s encoder as the vision tokenizer to generate discrete tokens of the given LQ image. The instruction is passed to the text tokenizer to generate text tokens, which are then concatenated with image tokens. Subsequently, the backbone transformer performs autoregressive prediction of the image degradation, semantic understanding and HQ image tokens. Finally, the output image tokens are passed to the vision de-tokenizer and decoded to the restored image.

as *degradation labels* during training. This phase provides quantitative degradation priors for subsequent phases.

Understanding. The phase of understanding constitutes a semantic-aware component in our PURE framework to extract and formalize contextual scene semantics from image content. To obtain these descriptions, we first utilize LLaVa [22] to generate structured textual descriptions of the ground-truth (GT) images of the LQ inputs. These semantic descriptions are then used to supervise the training of our PURE model by establishing text-visual correlations.

Restoration. The restoration phase synthesizes HQ images via autoregressive token generation, which is guided by 3 key elements: the degradation level, the semantic context, and the structural coherence of the evolving sequence. Integrating these elements, we ensure that the reconstructed image can not only address the degradation but also align with the semantics of the scene, resulting in content coherent and visually appealing Real-ISR outputs.

Training Loss. During training, we utilize the next-token prediction objective, optimizing a standard cross-entropy loss to jointly model the distribution of text and image tokens. The training loss is:

$$\mathcal{L} = \text{CrossEntropy}(y_t, p_\theta(x_t | x_{<t}, I, X_{LQ})), \quad (1)$$

where $p_\theta(x_t | x_{<t}, I, X_{LQ})$ represents the probability distribution of the model for generating the i -th token, conditioned on the input instruction I , LQ image tokens X_{LQ} , and all previously generated tokens $x_{<t}$.

3.4. Inference with Entropy-based Sampling

As mentioned in Sec. 3.1, we adapt the Top- k sampling strategy during inference. Specifically, a smaller k value restricts the sampling space and can preserve input image structures. In contrast, increasing k can result in images with richer details. Conventional approaches typically employ a global Top- k setting for all image tokens. However, in image restoration tasks, different regions exhibit varying requirements for detail richness. For example, areas with strong edges require fewer details, and a smaller k value is appropriate. Conversely, regions with fine textures (e.g., grasses, animal hairs) benefit from richer details, necessitating a larger k value. The challenge is then turned to how to determine the structural uncertainty of different image regions so that we can adaptively configure a tailored Top- k value for each image token.

In this work, we use entropy, a concept that can quantify uncertainty in probability distributions, as the uncertainty measure, which is defined as $H_t = -\sum_{i=1}^n p_i \log p_i$. By exploring the entropy of each token during generation, we observe a strong correlation between entropy and structural patterns of the generated image. As shown in Fig. 3, high-entropy tokens typically correspond to regions with complex structures or varied textures, while low-entropy tokens are often associated with areas with sharp edges. Based on this insight, we dynamically adjust the Top- k value based on the entropy of the current image token. The dynamic

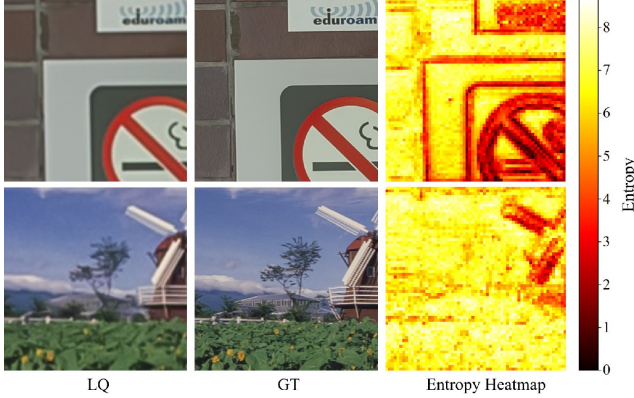


Figure 3. Visualization of entropy distribution in image token generation. The entropy heatmap shows token-wise uncertainty, where darker regions indicate higher entropy values and lighter regions represent lower entropy values.

Top- k value k_t at step t is calculated as:

$$k_t = k_{\min} + (k_{\max} - k_{\min}) \times \sigma(H_t - \mu), \quad (2)$$

where $\sigma(\cdot)$ is the sigmoid function, μ is the standard deviation of entropy observed during inference, and k_{\min} and k_{\max} are the predefined minimum and maximum values for Top- k sampling during image token generation. Our proposed entropy-based Top- k sampling strategy can balance fidelity and diversity in image token generation, significantly improving the perceptual quality of restored images, particularly in complex scenes with diverse spatial structures.

4. Experiments

4.1. Experimental Setup

Training Datasets. Following [39, 40], we train PURE on LSDIR [17] and a subset of 10,000 high-resolution facial images from FFHQ [13]. To generate realistic LQ-HQ image pairs for training, we apply the degradation pipeline from Real-ESRGAN [35], which introduces blur kernels, noise perturbations, and JPEG compression artifacts.

Test Datasets. For comprehensive evaluation of PURE, we employ one synthetic dataset and three real-world datasets for testing. (1) First, we resize the shortest side of the OST validation set [34] to 512 pixels and perform center-cropping to obtain 512×512 resolution images as the GTs. Using the same degradation pipeline as in SeeSR [40], we generate LQ-HQ image pairs, collectively referred to as OST-Val, which serves as our synthetic test set. (2) Second, we employ the real-world datasets RealSR [3] and RealLQ250 [2] for testing. (3) On the above three datasets, we perform $4 \times$ Real-ISR experiments as in most of the existing methods [39, 40, 43], where the LQ image is of 128×128 resolution. In this paper, we further evaluate PURE for $2 \times$ Real-ISR using the DrealSR [38] dataset to achieve a wider field of view that better aligns with real-world multi-object

Table 1. Comparative analysis of PSNR (dB) between the VAE used in SD-based methods and the VQGAN used in our PURE, with performance differences highlighted in red.

Tokenizers	OST-Val	RealSR	DrealSR
VAE	25.00	24.43	36.20
VQGAN	24.29 (-0.71)	23.53 (-0.90)	33.59 (-2.62)

scenarios. We center-crop the GT images from the DrealSR dataset to 512×512 while correspondingly center-cropping the LQ images to 256×256 .

Compared Methods. We compare PURE against state-of-the-art diffusion-based Real-ISR methods, including StableSR [33], PASD [43], DiffBIR [20], SeeSR [40] and OSediff [39]. All competing methods utilize comparable size training data, ensuring a fair comparison.

Evaluation Metrics. To holistically assess restoration quality, we employ a combination of reference-based and no-reference metrics. Pixel-level fidelity is measured through PSNR and SSIM [37] computed on the Y channel in YCbCr color space. Perceptual similarity is evaluated using LPIPS [48] and DISTS [7], which compare deep feature representations between restored and GT images. FID [11] quantifies the statistical distribution alignment between restored and reference images. For blind quality assessment without reference images, we incorporate NIQE [46], MANIQA [42], MUSIQ [14], CLIPQA [32] and TOPIQ [5] to evaluate image naturalness and structural integrity.

Implementation Details. We train PURE using the AdamW optimizer with an initial learning rate of 4×10^{-4} , following a cosine decay schedule during training. The model is trained on the entire dataset for 2 epochs with a batch size of 128, including a warmup phase spanning the first 0.5 epochs to stabilize early-stage optimization. Training is conducted on 512×512 resolution images with 32 NVIDIA A800 GPUs. During the inference process, the dynamic Top- k sampling parameters for image token generation are configured as $k_{\min} = 1$, $k_{\max} = 2000$ with $\mu = 5$, while a conservative Top- $k = 1$ strategy is implemented for text token generation to ensure optimal textual accuracy. We maintained the inference parameters used in Lumina-mGPT, setting CFG [21] to 0.8 and temperature to 0.9.

4.2. Comparison with State-of-the-Arts

Quantitative Comparisons.

In all of our competing methods, the variational auto-encoder (VAE) [25] is used to convert the input image into latent space for diffusion, while in our PURE, a VQGAN is used to convert images into discrete tokens for processing. Both VAE and VQGAN will lose image details, but VAE is more advantageous for its continuous representation. Tab. 1 quantify the fidelity (in terms of as PSNR) of GT images on the three test sets, which is actually the PSNR

Table 2. Quantitative comparison between PURE and state-of-the-art diffusion-based methods. The best and second best results of each metric are highlighted in **red** and **blue**, respectively.

Datasets	Methods	PSNR \uparrow	SSIM \uparrow	LPIPS \downarrow	DISTS \downarrow	FID \downarrow	NIQE \downarrow	MUSIQ \uparrow	MANIQA \uparrow	CLIPQA \uparrow	TOPIQ \uparrow
OST-Val	StableSR	19.97	0.4638	0.3367	0.2007	51.11	3.7669	74.38	0.6009	0.7194	0.7789
	DiffBIR	20.47	0.4694	0.3622	0.2059	61.28	4.5477	73.98	0.6377	0.7378	0.7983
	SeeSR	20.71	0.5004	0.3274	0.1935	56.32	3.9399	74.03	0.5920	0.6900	0.7945
	PASD	20.95	0.5053	0.4121	0.2190	66.92	4.8305	69.77	0.4289	0.5141	0.6307
	OSDiff	20.59	0.4954	0.3133	0.1926	52.11	3.8947	74.30	0.6102	0.6709	0.7755
	PURE	18.52	0.4181	0.3863	0.2052	55.19	4.7977	74.81	0.6424	0.7581	0.8148
RealSR	StableSR	24.64	0.7079	0.3004	0.2141	128.66	5.8823	72.19	0.4054	0.6234	0.6809
	DiffBIR	24.82	0.6495	0.3656	0.2400	131.01	5.8477	72.50	0.4729	0.7059	0.7313
	SeeSR	25.14	0.7210	0.3008	0.2224	125.61	5.3913	72.61	0.4203	0.6705	0.7354
	PASD	26.63	0.7660	0.2870	0.2034	125.26	5.9892	70.01	0.3382	0.4869	0.5988
	OSDiff	25.15	0.7341	0.2920	0.2127	123.73	5.6442	72.95	0.4507	0.6686	0.7106
	PURE	22.83	0.6079	0.3821	0.2458	188.33	5.4090	72.37	0.4527	0.6817	0.7165
DrealSR	StableSR	25.86	0.7380	0.2875	0.1951	95.71	5.9033	73.55	0.4399	0.7021	0.7408
	DiffBIR	26.82	0.7035	0.3389	0.2179	80.11	5.6977	73.23	0.5007	0.7225	0.7608
	SeeSR	27.71	0.7676	0.2768	0.2033	93.80	5.4440	73.45	0.4808	0.7046	0.7673
	PASD	29.73	0.8326	0.2099	0.1643	67.16	5.6899	72.40	0.4204	0.6268	0.6979
	OSDiff	26.60	0.7693	0.2633	0.1882	94.59	5.7724	73.98	0.4978	0.7114	0.7345
	PURE	24.73	0.6459	0.3452	0.2076	79.41	5.4846	73.28	0.5251	0.7259	0.7560

Table 3. Quantitative results on the RealLQ250 dataset. The best and second best results of each metric are highlighted in **red** and **blue**, respectively.

Methods	NIQE \downarrow	MUSIQ \uparrow	MANIQA \uparrow	CLIPQA \uparrow	TOPIQ \uparrow
StableSR	5.9122	73.75	0.5075	0.7273	0.7431
DiffBIR	4.7547	73.68	0.5971	0.7669	0.7629
SeeSR	4.2094	73.91	0.5241	0.7237	0.7621
PASD	4.3238	72.14	0.4388	0.6200	0.6578
OSDiff	4.1491	74.21	0.5263	0.7101	0.7285
PURE	4.5054	74.10	0.5409	0.7711	0.7751

upper bounds of Real-ISR performance. Taking DrealSR as an example, VAE outperforms VQGAN by 2.61 dB. Taking this fact into account, we investigate whether PURE, which relies on VQGAN for autoregressive token generation, can overcome this deficiency and show competitive Real-ISR performance.

Tabs. 2 and 3 presents a comprehensive quantitative comparison between PURE and state-of-the-art diffusion-based approaches on the four test datasets. (Note that RealLQ250 does not have GTs so that we can only compute the no-reference metrics.) Although PURE, as expected, show inferior results in full-reference based metrics such as PSNR, SSIM, *etc.*, it demonstrates highly competitive performance across no-reference metrics. This substantiates that PURE, via effective perception and understanding of the input LQ image, can exhibit robust image restoration capability and produce HQ images aligning with human visual preferences. We argue that this achievement is non-trivial considering the significant loss of details in the discrete tokenization process. On the other hand, such results imply the significant potentials of autoregressive multimodal gen-

erative models in real-world image restoration tasks.

Qualitative Comparison. We present qualitative comparisons with other Real-ISR methods in Fig. 4. As shown in the first case, our PURE approach successfully recovers the most authentic and accurate details, while the other methods yield either over-smoothed or incorrect textures. Similar observation can be found in the second case, where our approach generates more natural results with significantly reduced artifacts compared to the competing methods. For the remaining cases, PURE also shows advantages in terms of visual quality, producing more realistic texture details while maintaining better overall image fidelity. More visual results are provided in Appendix A.1.

User Study. To further evaluate the performance of competing methods, we conduct a user study. We randomly select 50 real-world LQ images from RealSR, DrealSR and RealLQ250, then employ PURE and five state-of-the-art diffusion-based Real-ISR approaches (StableSR, PASD, DiffBIR, SeeSR and OSDiff) to enhance them. These Real-ISR results, together with the LQ images, are presented to volunteers, who are asked to select the best restoration output based on two key criteria: 1) content consistency with the LQ input (including color fidelity, structural preservation, and texture accuracy); and 2) visual perceptual quality (encompassing natural appearance and richness of plausible details). Fifteen volunteers are invited to participate in the study, each making 50 pairwise comparisons over different methods. As demonstrated in Fig. 5, our PURE method achieves significantly better preference than diffusion-based methods, with a selection rate of 38.9%. This result demonstrates the great poten-

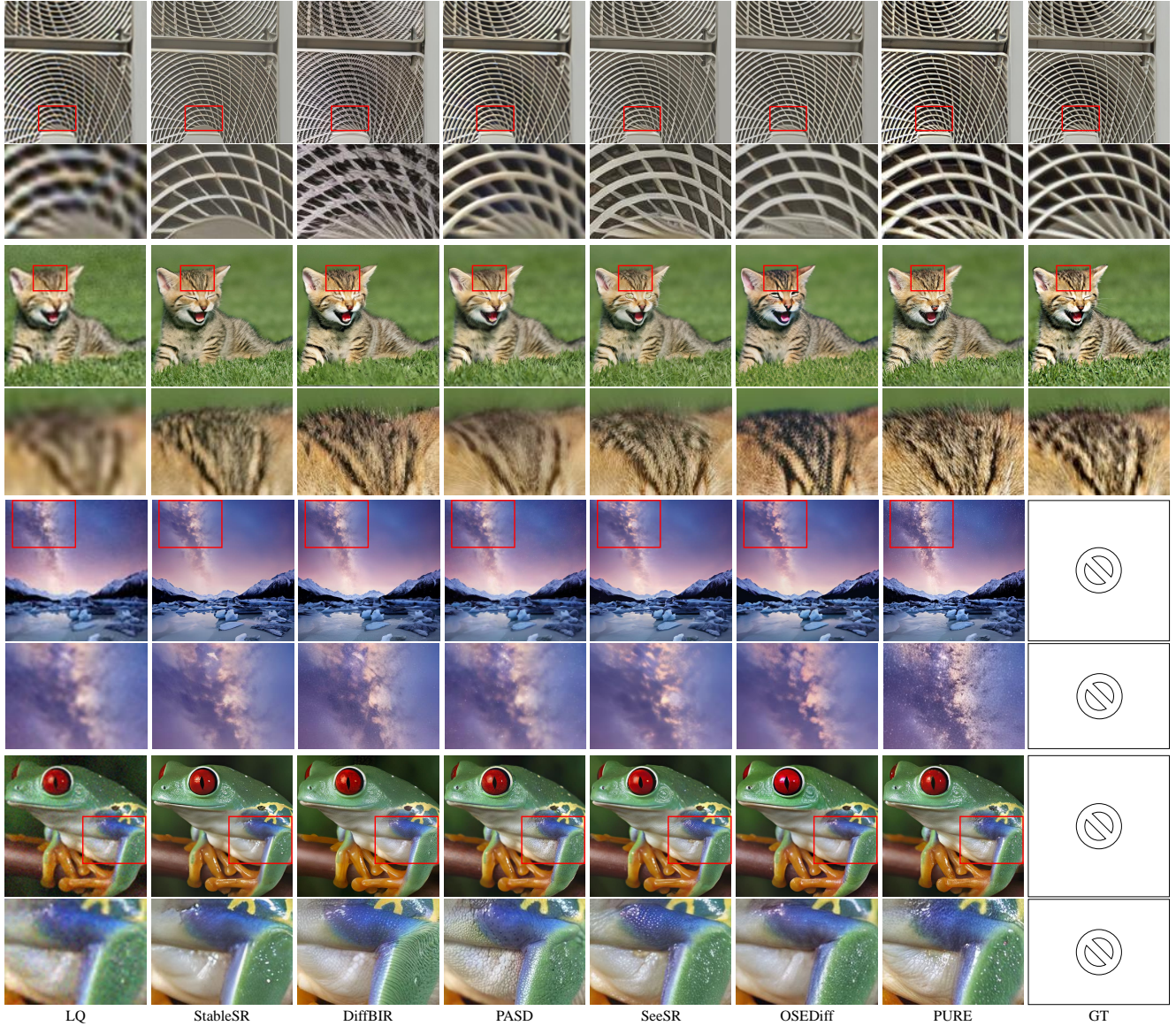


Figure 4. Qualitative comparisons of different Real-ISR methods. Please zoom in for a better view.

tial for autoregressive multi-modal models in solving real-world image restoration tasks.

Complexity Analysis. We then make a complexity comparison between PURE and the competing methods. As shown in Tab. 4, it is not a surprise that PURE, as an autoregressive multimodal generative model-based method, has much more parameters and significantly longer inference time than those SD-based methods. Specifically, the large amount of parameters are inherited from the Lumina-mGPT model, while the slower inference speed is determined by the sequential processing manner of autoregressive models, which predict the next-token one by one. In contrast, the SD-based approaches can perform diffusion denoising in parallel. However, it is worth mentioning our work is the

Table 4. Complexity comparison among different methods. All methods are tested with an input image of size 512×512 , and the inference time is measured on an A100 GPU.

	StableSR	DiffBIR	SeeSR	PASD	OSEDiff	PURE
Inference Time (s)	11.50	2.72	4.30	2.80	0.35	256.87
Total Param (M)	1410	1717	2524	1900	1775	7080

first one, to our best knowledge, which successfully applies the auto-regressive multimodal generative model to the task of Real-ISR and demonstrates its effectiveness.

4.3. Ablation Study

We perform ablation studies on our proposed perception-understanding strategy and the entropy-based Top- k sampling strategy. The visual comparisons for the ablation

Table 5. Ablation study on perception-understanding guidance mechanisms. The best results of each metric are marked in **bold**.

Strategy	PSNR \uparrow	SSIM \uparrow	LPIPS \downarrow	DISTS \downarrow	FID \downarrow	NIQE \downarrow	MUSIQ \uparrow	MANIQA \uparrow	CLIQQA \uparrow	TOPIQ \uparrow
<i>No Guidance</i>	23.43	0.5588	0.4452	0.2409	191.21	5.9722	73.23	0.4950	0.7202	0.7601
<i>Perception Guidance</i>	24.48	0.6510	0.3471	0.2106	83.20	5.5573	73.15	0.5189	0.7166	0.7410
<i>Understanding Guidance</i>	24.23	0.6282	0.3937	0.2244	141.05	5.6898	73.03	0.4955	0.7168	0.7493
<i>Full Guidance</i>	24.73	0.6459	0.3452	0.2076	79.41	5.4846	73.28	0.5251	0.7259	0.7560

Table 6. Ablation study on sampling strategies. The best results of each metric are marked in **bold**.

Strategy	PSNR \uparrow	SSIM \uparrow	LPIPS \downarrow	DISTS \downarrow	FID \downarrow	NIQE \downarrow	MUSIQ \uparrow	MANIQA \uparrow	CLIQQA \uparrow	TOPIQ \uparrow
<i>Top-1</i>	27.59	0.7945	0.2507	0.2173	115.39	7.9308	71.82	0.3779	0.5291	0.6313
<i>Top-2000</i>	24.56	0.6379	0.3619	0.2107	80.54	5.6159	73.38	0.5180	0.7169	0.7471
<i>Dynamic Top-k</i>	24.73	0.6459	0.3452	0.2076	79.41	5.4846	73.28	0.5251	0.7259	0.7560

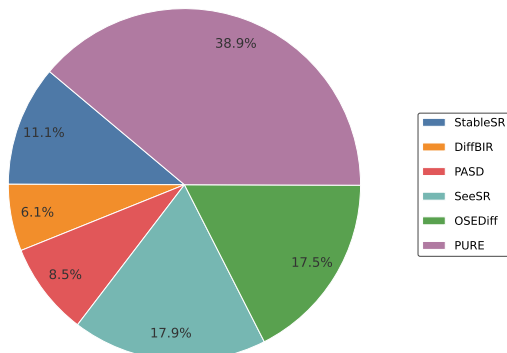


Figure 5. User study results on PURE and five state-of-the-art diffusion-based Real-ISR methods (StableSR, PASD, DiffBIR, SeeSR, OSEDiff) with 50 real-world images.

study are presented in Appendix A.2.

Perception-Understanding Guidance. To validate the effectiveness of our sequential perception-understanding-restoration paradigm, we systematically ablate the contribution of each text-guided component on DrealSR. The *Full Guidance* strategy strictly follows our paradigm, sequentially producing degradation scores, semantic descriptions, and restored images. *Perception Guidance* omits semantic captioning but retains degradation estimation, while *Understanding Guidance* removes degradation analysis to focus solely on semantic understanding. *No Guidance* bypasses all textual intermediates, directly mapping low-quality inputs to restored outputs. The results are shown in Tab. 5, from which we can have the following observations.

First, the *No Guidance* method under-performs on most metrics, particularly on reference-based metrics. In comparison, the *Perception Guidance* method shows significant improvements on reference-based metrics, especially PSNR (with a 1.05 dB increase), demonstrating the effectiveness of adaptive degradation perception for restoration. Meanwhile, *Understanding Guidance* achieves substantial improvements over *No Guidance* on reference-based metrics and some no-reference metrics (NIQE and MANIQA), proving that semantic understanding can help generate realistic details that better align with the original image’s semantics. Finally, *Full Guidance* attains the best perfor-

mance across most metrics. This hierarchy confirms that explicit degradation modeling enhances structural fidelity, semantic understanding drives realistic detail generation, and their integration through Full Guidance well balances physical accuracy and perceptual authenticity.

Entropy-based Top-k Sampling. We evaluate the proposed entropy-based dynamic Top-k sampling strategy against fixed Top-k baselines on DrealSR: 1) *Top-1*: Deterministic sampling ($k = 1$); 2) *Top-2000*: Maximal stochasticity ($k = 2000$). As quantified in Tab. 6, *Top-1* strategy achieves the best PSNR/SSIM metrics as it consistently selects the token with the highest probability, ensuring strong fidelity. However, it performs poorly on most other metrics due to the lack of diversity in generation. In contrast, the *Top-2000* strategy exhibits the worst PSNR/SSIM scores but outperforms *Top-1* on other metrics, benefiting from its diversity. The proposed Dynamic Top-k strategy strikes an effective balance between these two extremes. While achieving good PSNR and SSIM scores, it achieves the best performance on perceptual metrics (DISTS, FID) and no-reference metrics (NIQE, MUSIQ, MANIQA). This demonstrates that our dynamic Top-k sampling approach successfully navigates the trade-off between fidelity and perceptual quality, leveraging adaptive stochasticity to enhance the realism and naturalness of generated results without compromising much structural accuracy.

5. Conclusion and Limitation

We proposed PURE, a robust Real-ISR framework that integrated perception, understanding and restoration through instruction-tuning of the autoregressive multimodal generative model Lumina-mGPT. By jointly perceiving degradation strength, generating semantic descriptions, and restoring high-quality image tokens autoregressively, PURE addressed effectively the limitations of existing diffusion-based methods for handling complex scenes with semantic ambiguity and restoring unnatural local structures. The proposed entropy-based Top-k sampling strategy further improved local structure by adaptively adjusting token generation. Experiments showed that PURE effectively preserved

both global semantics and local details in challenging real-world scenarios, showcasing the potential of autoregressive multimodal paradigms for low-level vision tasks.

Limitations. Due to the large number of parameters in multimodal generative models and the nature of autoregressive model’s next-token prediction paradigm, PURE is large in size and slow in inference speed, limiting its application in many resource-constrained devices. In addition, VQGAN is employed as the vision decoder, whose reconstruction accuracy is lower than that of VAE in diffusion models. In future work, we plan to develop distillation techniques and explore parallel decoding strategies to improve computational efficiency, and investigate more effective vision encoders that can be adopted in autoregressive models.

References

- [1] Stability.ai. <https://stability.ai/stable-diffusion>. 1, 2
- [2] Yuang Ai, Xiaoqiang Zhou, Huaibo Huang, Xiaotian Han, Zhengyu Chen, Quanzeng You, and Hongxia Yang. Dreamclear: High-capacity real-world image restoration with privacy-safe dataset curation. In *The Thirty-eighth Annual Conference on Neural Information Processing Systems*, 2024. 5
- [3] Jianrui Cai, Hui Zeng, Hongwei Yong, Zisheng Cao, and Lei Zhang. Toward real-world single image super-resolution: A new benchmark and a new model. In *ICCV*, pages 3086–3095, 2019. 5
- [4] Bin Chen, Gehui Li, Rongyuan Wu, Xindong Zhang, Jie Chen, Jian Zhang, and Lei Zhang. Adversarial diffusion compression for real-world image super-resolution, 2024. 1, 2
- [5] Chaofeng Chen, Jiadi Mo, Jingwen Hou, Haoning Wu, Liang Liao, Wenxiu Sun, Qiong Yan, and Weisi Lin. Topiq: A top-down approach from semantics to distortions for image quality assessment. *IEEE Transactions on Image Processing*, 33:2404–2418, 2024. 5
- [6] Xiangyu Chen, Xintao Wang, Jiantao Zhou, Yu Qiao, and Chao Dong. Activating more pixels in image super-resolution transformer. In *Proceedings of the IEEE/CVF Conference on Computer Vision and Pattern Recognition*, pages 22367–22377, 2023. 1, 2
- [7] Keyan Ding, Kede Ma, Shiqi Wang, and Eero P Simoncelli. Image quality assessment: Unifying structure and texture similarity. *TPAMI*, 44(5):2567–2581, 2020. 5
- [8] Chao Dong, Chen Change Loy, Kaiming He, and Xiaoou Tang. Learning a deep convolutional network for image super-resolution. In *Computer Vision—ECCV 2014: 13th European Conference, Zurich, Switzerland, September 6–12, 2014, Proceedings, Part IV 13*, pages 184–199. Springer, 2014. 1, 2
- [9] Patrick Esser, Robin Rombach, and Bjorn Ommer. Taming transformers for high-resolution image synthesis. In *Proceedings of the IEEE/CVF conference on computer vision and pattern recognition*, pages 12873–12883, 2021. 3
- [10] Ian Goodfellow, Jean Pouget-Abadie, Mehdi Mirza, Bing Xu, David Warde-Farley, Sherjil Ozair, Aaron Courville, and Yoshua Bengio. Generative adversarial nets. In *NeurIPS*, 2014. 1
- [11] Martin Heusel, Hubert Ramsauer, Thomas Unterthiner, Bernhard Nessler, and Sepp Hochreiter. Gans trained by a two time-scale update rule converge to a local nash equilibrium. *NeurIPS*, pages 6626–6637, 2017. 5
- [12] Edward J Hu, Yelong Shen, Phillip Wallis, Zeyuan Allen-Zhu, Yuanzhi Li, Shean Wang, Lu Wang, and Weizhu Chen. Lora: Low-rank adaptation of large language models. *arXiv preprint arXiv:2106.09685*, 2021. 1
- [13] Tero Karras, Samuli Laine, and Timo Aila. A style-based generator architecture for generative adversarial networks. In *Proceedings of the IEEE/CVF conference on computer vision and pattern recognition*, pages 4401–4410, 2019. 5
- [14] Junjie Ke, Qifei Wang, Yilin Wang, Peyman Milanfar, and Feng Yang. Musiq: Multi-scale image quality transformer. In *Proceedings of the IEEE/CVF International Conference on Computer Vision*, pages 5148–5157, 2021. 5
- [15] Christian Ledig, Lucas Theis, Ferenc Huszár, Jose Caballero, Andrew Cunningham, Alejandro Acosta, Andrew Aitken, Alykhan Tejani, Johannes Totz, Zehan Wang, et al. Photo-realistic single image super-resolution using a generative adversarial network. In *Proceedings of the IEEE conference on computer vision and pattern recognition*, pages 4681–4690, 2017. 1, 2
- [16] Junnan Li, Dongxu Li, Caiming Xiong, and Steven Hoi. Blip: Bootstrapping language-image pre-training for unified vision-language understanding and generation. In *International Conference on Machine Learning*, pages 12888–12900. PMLR, 2022. 2
- [17] Yawei Li, Kai Zhang, Jingyun Liang, Jiezhong Cao, Ce Liu, Rui Gong, Yulun Zhang, Hao Tang, Yun Liu, Denis Deman-dolx, et al. Lsdirl: A large scale dataset for image restoration. In *Proceedings of the IEEE/CVF Conference on Computer Vision and Pattern Recognition*, pages 1775–1787, 2023. 5
- [18] Jingyun Liang, Jiezhong Cao, Guolei Sun, Kai Zhang, Luc Van Gool, and Radu Timofte. Swinir: Image restoration using swin transformer. In *ICCVW*, pages 1833–1844, 2021. 1, 2
- [19] Bee Lim, Sanghyun Son, Heewon Kim, Seungjun Nah, and Kyoung Mu Lee. Enhanced deep residual networks for single image super-resolution. In *Proceedings of the IEEE conference on computer vision and pattern recognition workshops*, pages 136–144, 2017. 1, 2
- [20] Xinqi Lin, Jingwen He, Ziyang Chen, Zhaoyang Lyu, Ben Fei, Bo Dai, Wanli Ouyang, Yu Qiao, and Chao Dong. Diffbir: Towards blind image restoration with generative diffusion prior. *arXiv preprint arXiv:2308.15070*, 2023. 1, 5
- [21] Dongyang Liu, Shitian Zhao, Le Zhuo, Weifeng Lin, Yu Qiao, Hongsheng Li, and Peng Gao. Lumina-mgpt: Illuminate flexible photorealistic text-to-image generation with multimodal generative pretraining, 2024. 2, 3, 5
- [22] Haotian Liu, Chunyuan Li, Qingyang Wu, and Yong Jae Lee. Visual instruction tuning. In *NeurIPS*, 2023. 2, 4
- [23] Chong Mou, Xintao Wang, Yanze Wu, Ying Shan, and Jian Zhang. Empowering real-world image super-resolution with

- flexible interactive modulation. *IEEE Transactions on Pattern Analysis and Machine Intelligence*, 46(11):7317–7330, 2024. 3
- [24] Alec Radford, Jong Wook Kim, Chris Hallacy, Aditya Ramesh, Gabriel Goh, Sandhini Agarwal, Girish Sastry, Amanda Askell, Pamela Mishkin, Jack Clark, et al. Learning transferable visual models from natural language supervision. In *International conference on machine learning*, pages 8748–8763. PMLR, 2021. 2
- [25] Robin Rombach, Andreas Blattmann, Dominik Lorenz, Patrick Esser, and Björn Ommer. High-resolution image synthesis with latent diffusion models, 2021. 5
- [26] Noam Shazeer. Glu variants improve transformer, 2020. 3
- [27] Jianlin Su, Yu Lu, Shengfeng Pan, Ahmed Murtadha, Bo Wen, and Yunfeng Liu. Roformer: Enhanced transformer with rotary position embedding, 2023. 3
- [28] Lingchen Sun, Rongyuan Wu, Zhiyuan Ma, Shuaizheng Liu, Qiaosi Yi, and Lei Zhang. Pixel-level and semantic-level adjustable super-resolution: A dual-lora approach, 2024. 1, 2
- [29] Peize Sun, Yi Jiang, Shoufa Chen, Shilong Zhang, Bingyue Peng, Ping Luo, and Zehuan Yuan. Autoregressive model beats diffusion: Llama for scalable image generation. *arXiv preprint arXiv:2406.06525*, 2024. 3
- [30] Chameleon Team. Chameleon: Mixed-modal early-fusion foundation models. *arXiv preprint arXiv:2405.09818*, 2024. 2, 3
- [31] Hugo Touvron, Thibaut Lavril, Gautier Izacard, Xavier Martinet, Marie-Anne Lachaux, Timothée Lacroix, Baptiste Rozière, Naman Goyal, Eric Hambro, Faisal Azhar, Aurelien Rodriguez, Armand Joulin, Edouard Grave, and Guillaume Lample. Llama: Open and efficient foundation language models, 2023. 2
- [32] Jianyi Wang, Kelvin CK Chan, and Chen Change Loy. Exploring clip for assessing the look and feel of images. In *Proceedings of the AAAI Conference on Artificial Intelligence*, pages 2555–2563, 2023. 5
- [33] Jianyi Wang, Zongsheng Yue, Shangchen Zhou, Kelvin CK Chan, and Chen Change Loy. Exploiting diffusion prior for real-world image super-resolution. *arXiv preprint arXiv:2305.07015*, 2023. 1, 5
- [34] Xintao Wang, Ke Yu, Chao Dong, and Chen Change Loy. Recovering realistic texture in image super-resolution by deep spatial feature transform. In *Proceedings of the IEEE conference on computer vision and pattern recognition*, pages 606–615, 2018. 5
- [35] Xintao Wang, Liangbin Xie, Chao Dong, and Ying Shan. Real-esrgan: Training real-world blind super-resolution with pure synthetic data. In *ICCVW*, pages 1905–1914, 2021. 1, 2, 5
- [36] Xinlong Wang, Xiaosong Zhang, Zhengxiong Luo, Quan Sun, Yufeng Cui, Jinsheng Wang, Fan Zhang, Yueze Wang, Zhen Li, Qiying Yu, et al. Emu3: Next-token prediction is all you need. *arXiv preprint arXiv:2409.18869*, 2024. 2
- [37] Zhou Wang, Alan C Bovik, Hamid R Sheikh, and Eero P Simoncelli. Image quality assessment: from error visibility to structural similarity. *IEEE transactions on image processing*, 13(4):600–612, 2004. 5
- [38] Pengxu Wei, Ziwei Xie, Hannan Lu, Zongyuan Zhan, Qixiang Ye, Wangmeng Zuo, and Liang Lin. Component divide-and-conquer for real-world image super-resolution. In *ECCV*, pages 101–117, 2020. 5
- [39] Rongyuan Wu, Lingchen Sun, Zhiyuan Ma, and Lei Zhang. One-step effective diffusion network for real-world image super-resolution. *arXiv preprint arXiv:2406.08177*, 2024. 1, 2, 5
- [40] Rongyuan Wu, Tao Yang, Lingchen Sun, Zhengqiang Zhang, Shuai Li, and Lei Zhang. Seesr: Towards semantics-aware real-world image super-resolution. In *CVPR*, 2024. 1, 2, 5
- [41] Jinheng Xie, Weijia Mao, Zechen Bai, David Junhao Zhang, Weihao Wang, Kevin Qinghong Lin, Yuchao Gu, Zhijie Chen, Zhenheng Yang, and Mike Zheng Shou. Show-o: One single transformer to unify multimodal understanding and generation. *arXiv preprint arXiv:2408.12528*, 2024. 2
- [42] Sidi Yang, Tianhe Wu, Shuwei Shi, Shanshan Lao, Yuan Gong, Mingdeng Cao, Jiahao Wang, and Yujiu Yang. Maniqa: Multi-dimension attention network for no-reference image quality assessment. In *CVPR*, pages 1191–1200, 2022. 5
- [43] Tao Yang, Rongyuan Wu, Peiran Ren, Xuansong Xie, and Lei Zhang. Pixel-aware stable diffusion for realistic image super-resolution and personalized stylization. *arXiv preprint arXiv:2308.14469*, 2023. 1, 2, 5
- [44] Fanghua Yu, Jinjin Gu, Zheyuan Li, Jinfan Hu, Xiangtao Kong, Xintao Wang, Jingwen He, Yu Qiao, and Chao Dong. Scaling up to excellence: Practicing model scaling for photo-realistic image restoration in the wild. In *CVPR*, 2024. 1, 2
- [45] Biao Zhang and Rico Sennrich. Root Mean Square Layer Normalization. In *Advances in Neural Information Processing Systems 32*, Vancouver, Canada, 2019. 3
- [46] Lin Zhang, Lei Zhang, and Alan C Bovik. A feature-enriched completely blind image quality evaluator. *TIP*, 24(8):2579–2591, 2015. 5
- [47] Lvmin Zhang, Anyi Rao, and Maneesh Agrawala. Adding conditional control to text-to-image diffusion models. In *ICCV*, pages 3836–3847, 2023. 1, 2
- [48] Richard Zhang, Phillip Isola, Alexei A Efros, Eli Shechtman, and Oliver Wang. The unreasonable effectiveness of deep features as a perceptual metric. In *CVPR*, pages 586–595, 2018. 5
- [49] Yulun Zhang, Kunpeng Li, Kai Li, Lichen Wang, Bineng Zhong, and Yun Fu. Image super-resolution using very deep residual channel attention networks. In *Proceedings of the European conference on computer vision (ECCV)*, pages 286–301, 2018. 1, 2
- [50] Chunting Zhou, Lili Yu, Arun Babu, Kushal Tirumala, Michihiro Yasunaga, Leonid Shamis, Jacob Kahn, Xuezhe Ma, Luke Zettlemoyer, and Omer Levy. Transfusion: Predict the next token and diffuse images with one multi-modal model. 2024. 2

A. Appendix

In the appendix, we first present more visual comparisons of the competing Real-ISR methods, then present the visual results in our ablation study.

A.1. More Visual Comparisons

We present more visual comparisons with state-of-the-art diffusion-based Real-ISR methods on real-world images. As illustrated in Fig. 6 and Fig. 7, our proposed PURE demonstrates superior restoration quality across diverse scenarios, including animals, plants, humans, and landscapes. The PURE framework not only effectively preserves the structural and textural integrity of LQ input images, but also generates more abundant and plausible details, achieving exceptional visual quality.

A.2. Visual Results for Ablation Study

We provide visual comparison results for the ablation studies conducted in the main paper.

Perception-Understanding Guidance. We first present visual comparisons on perception-understanding guidance, as illustrated in Fig. 8. The *No Guidance* method demonstrates suboptimal restoration results with noticeable degradation in both cases, mainly due to its sole reliance on the LQ input image as the conditioning factor. Both *Perception Guidance* and *No Guidance* fail to generate rich details due to the absence of semantic description guidance. The *Understanding Guidance* produces erroneous details (*e.g.*, eyelashes), which can be attributed to the lack of adaptive degradation awareness. The *Full Guidance* achieves the best restoration quality among all variants.

Entropy-based Top- k Sampling. To demonstrate the effectiveness of our proposed entropy-based Top- k sampling strategy, we present visual comparison results by applying both fixed and dynamic Top- k sampling approaches. As illustrated in Fig. 9, the *Top-1* strategy yields the smoothest yet most blurry restoration results, as its generative capability is constrained by selecting only the most probable image token at each step. In contrast, while the *Top-2000* approach generates more details, it produces inferior visual perception quality with more erroneous textures. Notably, our entropy-based Top- k sampling achieves the best restoration quality, maintaining superior fidelity while generating more realistic and authentic details.

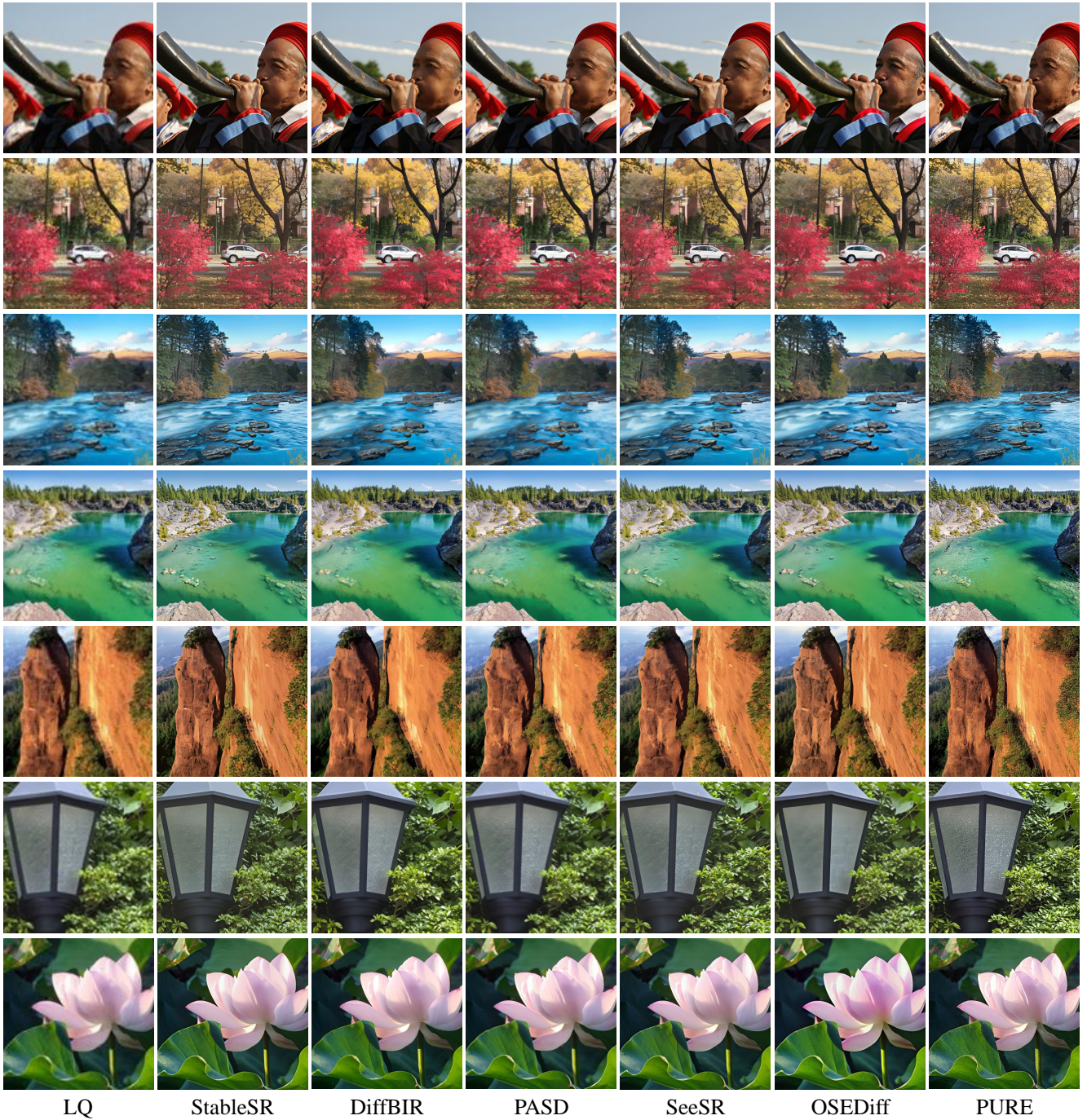


Figure 6. Visual comparisons of different Real-ISR methods on real-world images. Please zoom in for a better view.



Figure 7. Visual comparisons of different Real-ISR methods on real-world images. Please zoom in for a better view.



Figure 8. Visual comparisons for perception-understanding guidance ablation. Please zoom in for a better view.

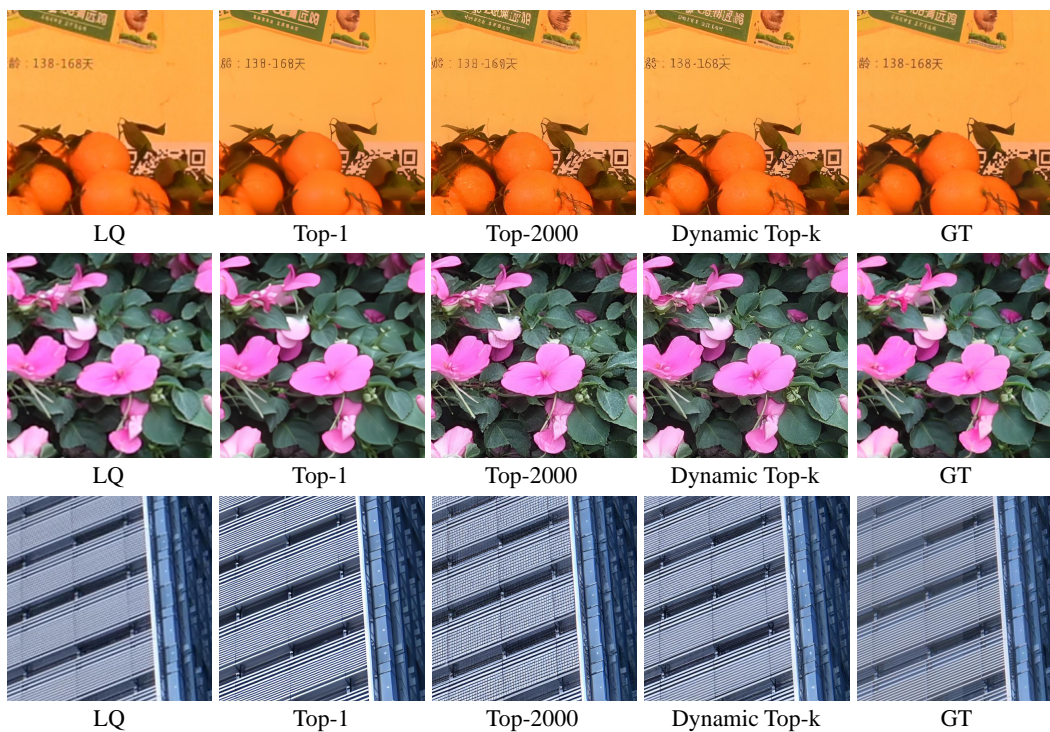


Figure 9. Visual comparisons for entropy-based Top- k sampling ablation. Please zoom in for a better view.